30. Buckley, G. B., Brochu, C. B., Krause, D. W. & Pol, D. A pug-nosed crocodyliform from the Late Cretaceous of Madagascar. *Nature* **405,** 941–944 (2000).
31. Swofford, D. L. *PAUP*: Phylogenetic Analysis Using Parsimony (* and Other Methods)* Version 4.0b2a. (Sinauer, Sunderland, 1999).

Supplementary information is available on *Nature*'s World-Wide Web site (http://www.nature.com) or as paper copy from the London editorial office of *Nature*.

Acknowledgements

'Misaotra betsika' to the villagers of Berivotra, Madagascar. M. Hallet provided the illustrations and M. Stewart and T. Ready took the photographs. Thanks to R. Rogers, D. Krause, M. O'Leary, R. Coria and P. Upchurch for comments and discussion. Funding was provided by NSF, National Geographic Society, Jurassic Foundation, GSA and the Gabor Inke Graduate Student Fellowship.

Correspondence and requests for materials should be addressed to K.C.R. (e-mail: krogers@smm.org).

Neanderthal cranial ontogeny and its implications for late hominid diversity

Marcia S. Ponce de León & Christoph P. E. Zollikofer

Anthropologisches Institut and Institut für Informatik/MultiMedia Laboratorium Universität Zürich-Irchel, Winterthurerstrasse 190, CH-8057 Zürich, Switzerland
The authors contributed equally to this work

Homo neanderthalensis **has a unique combination of craniofacial features that are distinct from fossil and extant 'anatomically modern'** ***Homo sapiens*** **(modern humans). Morphological evidence, direct isotopic dates[1] and fossil mitochondrial DNA from three Neanderthals[2,3] indicate that the Neanderthals were a separate evolutionary lineage for at least 500,000 yr. However, it is unknown when and how Neanderthal craniofacial autapomorphies (unique, derived characters) emerged during ontogeny. Here we use computerized fossil reconstruction[4] and geometric morphometrics[5,6] to show that characteristic differences in cranial and mandibular shape between Neanderthals and modern humans arose very early during development, possibly prenatally, and were maintained throughout postnatal ontogeny. Postnatal differences in cranial ontogeny between the two taxa are characterized primarily by heterochronic modifications of a common spatial pattern of development. Evidence for early ontogenetic divergence together with evolutionary stasis of taxon-specific patterns of ontogeny is consistent with separation of Neanderthals and modern humans at the species level.**

Comparative analyses of immature crania indicate that diagnostic Neanderthal characters appeared early during ontogeny[7,8] and that the Neanderthal ontogenetic process was fast relative to that of the modern humans[7,9–11]. Here, we use a new methodological approach to study the comparative ontogeny of Neanderthal and modern human skulls. After computerized reconstruction of fragmentary fossil specimens[4,12–14], we applied geometric morphometric methods (GMM)[5] to identify and visualize complex patterns of morphological change during ontogeny (see Methods). In GMM the form of a specimen is described by the spatial configuration of a set of three-dimensional anatomical landmarks. Size-corrected variation in shape can then be computed in terms of between-specimen rearrangements of landmark positions. To capture large trends in shape variation in ontogenetic samples of Neanderthals and modern humans, we used relative warp analysis[5,6], which separates shape variability into statistically independent factors. Each relative warp thus captures an independent aspect of shape variation in the sample (Fig. 1) that can be plotted ontogenetically as temporal (Fig. 2) and spatial (Figs 3 and 4) patterns of morphological change.

Our relative warp analyses are based on a large cross-sectional ontogenetic series of Neanderthal cranial and mandibular specimens that were reconstructed by computerized methods, and a comparative fossil/recent modern human sample. The Neanderthal sample mostly comprises individuals from dental stage 3 (3–6 yr) to adulthood, but includes an early postnatal mandible (Amud 7, about 0.5 yr[8]) and a cranium and mandible from dental stage 2 (Pech de l'Azé, about 2.5 yr); the modern human sample includes individuals from all ontogenetic stages—from perinatal through to adulthood (see Methods and Supplementary Information for sample details and landmark definitions). We computed the statistically independent relative warps for the combined craniomandibular landmark configurations (Fig. 1a) and for cranial and mandibular configurations in isolation (Fig. 1b, c), and plotted these against three additional factors: (1) individual age (dental

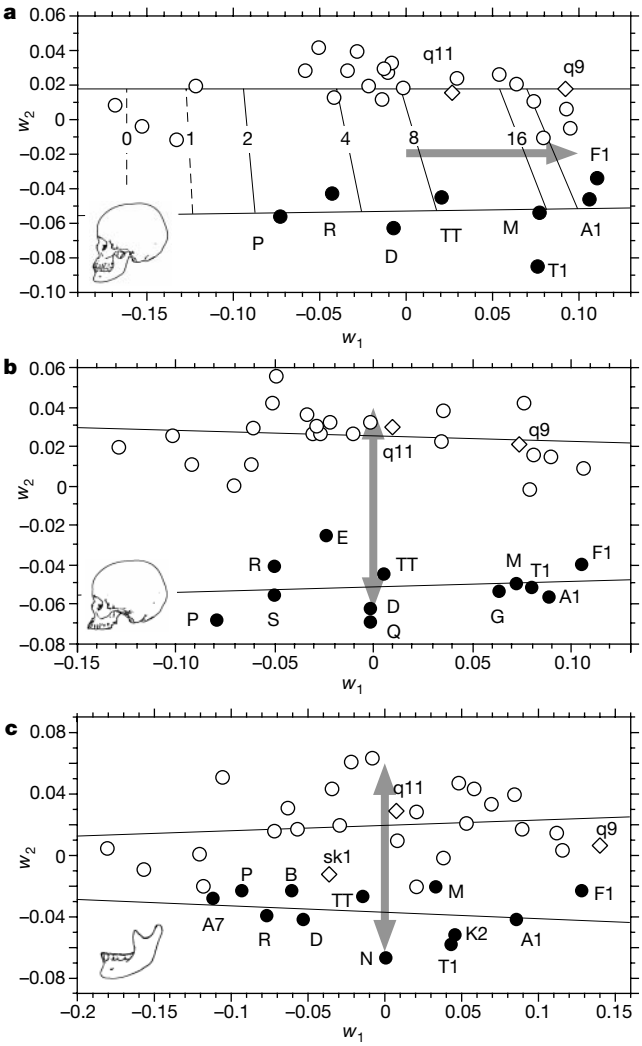

Figure 1 Shape variability in an ontogenetic series of Neanderthals (filled circles; see Methods for specimen labels) and modern humans (open circles/diamonds indicate extant/fossil specimens, respectively) for craniomandibular (**a**), cranial (**b**) and mandibular (**c**) landmark configurations. The labels w_1 and w_2 represent factors of shape variation resulting from relative warp analysis[5,6]. Neanderthals and modern humans follow ontogenetic trajectories that are approximately parallel (lines are principal axes of within-taxon correlation). The arrow in **a** characterizes the shared Neanderthal/modern human mode of development as shown in Fig. 3; taxon-specific trajectories are connected with lines at dental ages 0 (birth), 1, 2, 4, 8, 16 yr and adulthood. Arrows in **b** and **c** indicate differences in shape between Neanderthals and modern humans as shown in Fig. 4.

age); (2) centroid size (S, the extent of the landmark configuration); and (3) taxon (Neanderthal compared to modern human).

In all three analyses, only the first two statistically independent relative warps (w_1 and w_2) covary significantly with age, S and taxon, which together account for about 60% of the total shape variability (see Methods and Supplementary Information for details of relative warp analysis). There are clear patterns of covariation: w_1 describes shape variation related to size and age (Figs 1 and 2), whereas w_2 describes taxon-specific shape variation (Fig. 1). Each w_1–w_2 coordinate in Fig. 1 corresponds to a specific morphological configuration in physical space, and each vector (arrows along statistically independent relative warps in Fig. 1) indicates a distinct spatial pattern of morphological change. The most important result of the analyses (evident from Fig. 1) is that taxon-specific differences in craniomandibular shape are present by dental stage 2 and remain subsequently unchanged during ontogeny. This indicates that the characteristic morphologies that distinguish both Neanderthals and modern humans develop before dental stage 2, during early postnatal or possibly during prenatal ontogeny. From dental stage 2 onwards, Neanderthals and modern humans follow parallel ontogenetic trajectories along the direction of w_1 (Fig. 1), demonstrating a shared spatial pattern of morphological change (Fig. 3). The different lengths of the trajectories in Fig. 1, however, indicate that there are heterochronic differences between the taxa in their postnatal ontogeny. Plots of the relationship between dental age, craniomandibular shape w_1 and size S (Fig. 2) show that although the two taxa follow similar ontogenetic allometries (Fig. 2a), Neanderthals compared to modern humans show rate hypermorphosis (faster rates of growth and development leading to greater adult values of size and shape) during ontogeny (Fig. 2b, c). In all analyses, the fossil modern human subsample falls within the range of ontogenetic variability displayed by the extant modern human sample. In addition, the Neanderthals analysed here, which sample a long period of time[1], exhibit similar within-taxon ontogenetic variability, suggesting long-term stability of the modern human and Neanderthal patterns of ontogeny.

To further explore taxon-specific regional differences in cranial and mandibular growth, Figs 3 and 4 express statistically independent factors w_1 and w_2 as modifications of the Neanderthal/modern human consensus morphology (computed from a 5-year-old modern human specimen). Components of shape change were computed perpendicular and parallel to the craniomandibular surface and were visualized, respectively, using colours and vector fields (see Methods). Figure 3 shows the shared Neanderthal/modern human pattern of craniomandibular shape change from dental stage 2 to adulthood. The stability of this pattern over an extended phase of ontogeny (linear trajectories in Fig. 1a) indicates that the spatial distribution of areas of bone deposition/resorption and the relative rates of growth in these areas were constant in both taxa[15]. Patterns of Neanderthal and modern human ontogeny from dental stage 2 onwards therefore apparently derive from generally similar growth processes.

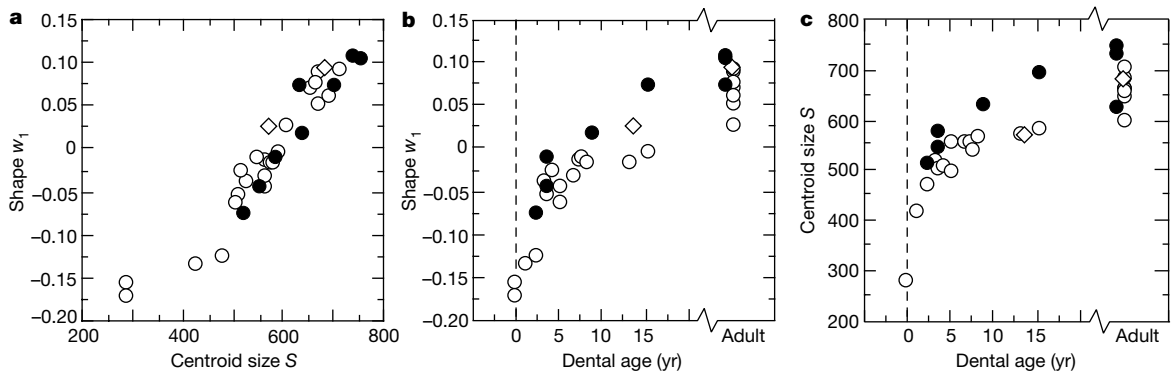

Figure 2 Correlations between shape (w_1), centroid size S and dental age (in postnatal years) for craniomandibular morphologies of Neanderthals (filled circles) and extant/fossil modern humans (open circles/diamonds, respectively). **a**, Ontogenetic allometry (w_1 versus S). **b**, Development (w_1 versus dental age). **c**, Growth (S versus dental age). Compared to modern humans, Neanderthals show rate hypermorphosis during development and growth.

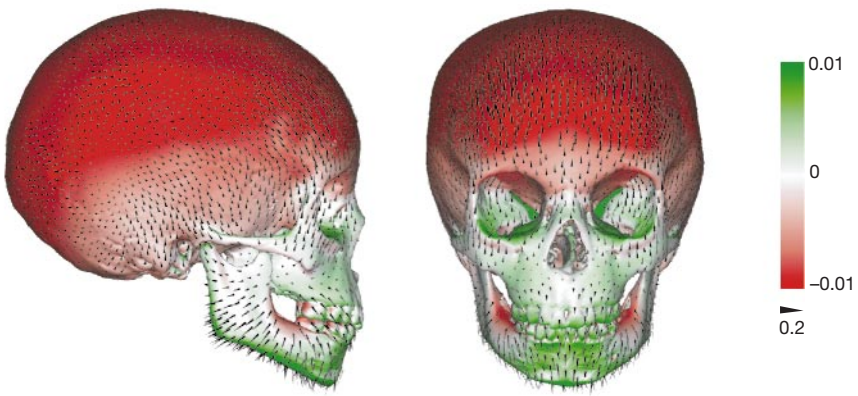

Figure 3 Patterns of shape change during postnatal development in Neanderthals and modern humans. A Neanderthal/modern human consensus skull is shown. Changes in morphology (corresponding to transformation along the arrow in Fig. 1a) are visualized with colours and vector fields (see Methods). Red and green indicates direction (inward and outward, respectively) and magnitude of shape change perpendicular to the surface of the skull. Arrows indicate direction and magnitude of shape change tangential to the surface (all scales in units of centroid size, S). Note the projection and downward elongation of the face and mandible, as opposed to the relative 'contraction' of the cranial vault (size S is held constant).

Figure 4 shows quantitative differences between Neanderthal and modern human morphologies that are already established at dental stage 2 and that are consistent with previous characterizations of the differences between the taxa[1,8,16–19]. Relative to modern humans, Neanderthals have a low cranial vault that is expanded posterolaterally. The boundary between superior and inferior regions of the vault (as visualized by colour in Fig. 4a–c) probably corresponds to the circumcranial reversal line that separates depository from resorptive growth fields on the internal surface of the braincase[20]. Increased drift and displacement in the inferior region of the Neanderthal cranial vault may therefore account for many of the Neanderthal apomorphies (derived characters) found, such as a broadened temporal region, rounded lateral cranial walls[1], a more caudal position of the middle cranial fossa, an elongated foramen magnum[8], and a large occipital squama[21] (Fig. 4a–c). The differences in growth fields that may account for these features probably reflect taxon-specific differences in interactions between cranial base shape and brain size/shape during early development[21].

Differential activity of growth fields may also explain many unique aspects of Neanderthal maxillofacial and mandibular morphology (Fig. 4d–f). In the fetal/early postnatal mandible, the lingual surfaces of the corpus and the external and anterior surfaces of the rami are resorptive[20], such that differential growth patterns affect the inclination of the rami relative to the cranial midplane and their anteroposterior position relative to the dentition. Visualization of relative warp analyses suggests that, compared to modern humans, the Neanderthal mandible was characterized by relatively less mediolateral growth and more anteroposterior growth: the rami are relatively inclined (having short condylar processes that are positioned laterally), and the corpus and rami are at a posterior position relative to the dentition (suggesting an early rather than late[19] ontogenetic origin of the retromolar space[16,17,22]). In humans, depository growth fields in the most anterior regions of the maxilla and mandible turn into resorptive fields shortly after birth, limiting facial projection during postnatal ontogeny[20,23]. According to our data, Neanderthals follow a similar postnatal pattern. Thus,

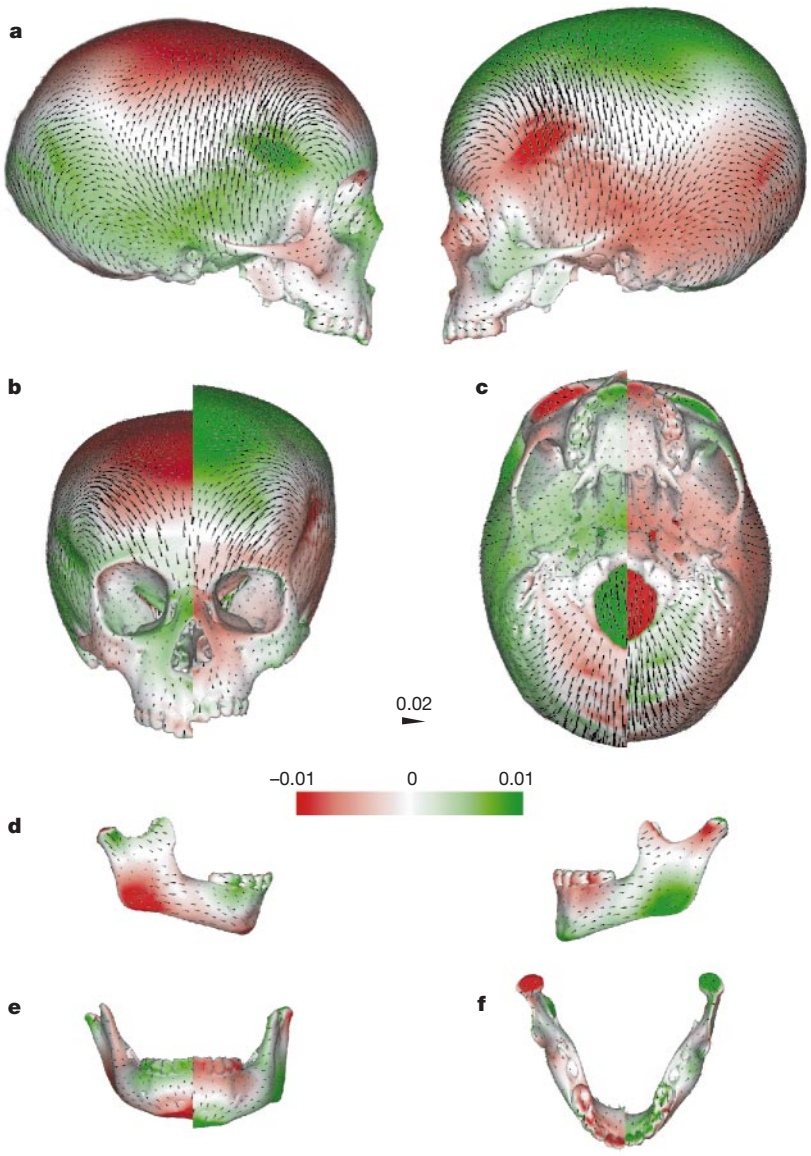

Figure 4 Shape differences between Neanderthal and modern human skulls (**a**–**c**) and mandibles (**d**–**f**). Left panels show Neanderthal morphologies; right panels show modern human morphologies (corresponding to opposite tips of the arrows in Fig. 1b, c). The patterns of colour indicate the direction and magnitude of shape difference of each taxon relative to the other and can tentatively be interpreted as representing contrasts between modes of prenatal (and early postnatal) development. Red and green indicates shape differences perpendicular (inward and outward, respectively) to the cranial and mandibular surfaces. Arrows indicate differences tangential to surfaces (all scales in units of centroid size, *S*). An animated version (Neanderthal–modern human transition) is available as Supplementary Information.

increased rates of fetal growth and/or later reversal of growth fields may be responsible for many characteristic aspects of Neanderthal midfacial prognathism, such as expanded maxillae, a spacious nasal cavity, a receding cheek region (Fig. 4a–c), and a longer persistence of the premaxillary suture[24]. Similar differences may generate the receding symphyseal region of the Neanderthal mandible.

The above analyses therefore indicate that most of the principal differences between Neanderthal and modern human skulls result from ontogenetically early differences in the relative timing and rates of activity at specific growth fields. These data thus support recent studies suggesting that early modifications of growth processes, notably in basicranial morphogenesis, have a principal role in generating evolutionary novelty in the hominid cranium[21,23,25,26]. Pronounced basicranial flexion at the spheno-occipital synchondrosis before 2 yr accounts for the unique position of the modern human face beneath the anterior cranial fossa[23,27]. It is therefore probable that the midfacial projection that is characteristic of Neanderthals[16–18] (Fig. 4a, b) results, in part, from less basicranial flexion during early postnatal or possibly prenatal ontogeny[23]. The early appearance of taxon-specific features between Neanderthals and modern humans, the morphological distinctiveness of these taxa throughout later postnatal ontogeny, and the evidence for evolutionary stasis of taxon-specific patterns of ontogeny, all support the theory[8,12,18,25] that *Homo neanderthalensis* and *Homo sapiens* represent morphologically discrete, separate species, which belonged to distinct evolutionary lineages[28]. It remains to be tested whether the observed pattern of evolutionary developmental diversification—prenatal divergence in conjunction with postnatal parallelism of developmental patterns—is characteristic for hominid evolution in general. □

Methods

Sample structure

The Neanderthal sample comprises 11 immature and 5 adult specimens, respectively: Amud 7 (A7; 0.5 yr); Pech de l'Azé (P; 2.2 yr); Barakai (B; 3 yr); Subalyuk 2 (S; 3.2 yr); Roc de Marsal (R; 3.5 yr); Devil's Tower (Gibraltar 2) (D; 3.5 yr); Engis 2 (E; 5.5 yr); La Quina 18 (Q; 6.5 yr); Teshik Tash (TT; 8.5 yr); La Naulette (N; 14 yr); Le Moustier 1 (M; 15 yr), all or which are immature; and Amud 1 (A1); La Ferrassie 1 (F1); Forbes' Quarry (Gibraltar 1) (G); Kebara 2 (K2); and Tabun 1 (T1), which are adult specimens. The fossil modern human sample comprises 3 specimens from the Near East: Skhul 1 (sk1; 3.5 yr); Qafzeh 11 (q11; 13.5 yr); and Qafzeh 9 (q9; adult), all of which are dated to about 100,000 yr ago[1]. The extant modern humans are represented by a pooled-sex sample of 22 specimens from Europe, Africa, Asia, America and Australia. This sample includes hyper-robust specimens from high north/south latitudes (for details see Supplementary Information Table 1).

Ageing

We estimated ages at death of both Neanderthal and modern human specimens with modern standard scores of dental eruption[29]; we used ages based on perikymata where available[9]. Direct age estimates based on perikymata indicate that application of modern human dental scores may bias results towards higher ages in Neanderthals[9]. As Neanderthal cranial ontogeny tends to be slightly fast relative to modern humans[7,9,10], dental scoring yields conservative estimates for individual ages. To distinguish early versus late phases of postnatal ontogeny, we discern between dental stage 2 (after eruption of dc (lower deciduous canine) and before full crown development of I1) and dental stage 3 (crown of I1 fully developed and before eruption of M1).

Data acquisition and fossil reconstruction

After acquisition of volume data with computer tomography, we generated three-dimensional, graphical object representations of all specimens. We reconstructed the fossil specimens by using special-purpose virtual reality tools[30]. Briefly, filling material was removed from earlier reconstructions, the isolated fossil fragments were re-composed on the computer screen, missing parts were completed with mirror-imaged counterparts, and taphonomic deformation was tentatively corrected, using the methods and anatomical criteria described elsewhere[4,12,14].

Landmark data registration

Three-dimensional coordinates of the anatomical landmarks were determined on the graphical representations of the specimens. Virtual registration allows landmark data acquisition on external and internal cranial surfaces[4]. The data set used in GMM analysis comprises 51 cranial (15 midsagittal and 18 bilateral pairs) and 22 mandibular (4 midsagittal and 9 bilateral pairs) landmarks (for details see Supplementary Information Table 2). All landmarks were chosen to represent locations of between-specimen homology.

Analysis of shape variability

Relative warp analysis provides an effective means to detect and analyse patterns of correlated shape change in multi-landmark configurations. We performed relative warp analysis according to methods in ref. 6. To constrain modes of shape variation to bilateral symmetry, each specimen's landmark configuration was made symmetrical by generalized least-squares (GLS) superimposition with its mirror-imaged counterpart, and subsequent averaging. The form of each specimen is defined as the set of its three-dimensional landmark coordinates. As a linear measure of size, centroid size S is used, calculated as the square root of the sum of squared distances of all landmarks from the centre of gravity (the centroid) of the landmark configuration[5]. GLS fitting of the size-normalized ($S = 1$) landmark configurations of all specimens yields an average configuration (the consensus) and defines a linearized Procrustes space in which the shape of each specimen is given by its linear deviation (landmark by landmark) from the consensus. Using the thin plate spline (TPS) eigenfunctions of the consensus, each specimen is then expressed as a smooth deformation of the consensus, given by its partial warp scores[5]. An array of orthogonal basis vectors, the relative warps, were calculated to reduce the dimensionality of the resulting partial warp space. Relative warps are statistically independent factors of shape variation that account for the largest, second largest and successively smaller proportions of the total sample variance in shape (for details see Supplementary Information Table 3).

Visualization of shape change

As relative warps are TPS functions, each point in the space of relative warps (see Fig. 1) corresponds to one specific physical landmark configuration resulting from a deformation of the consensus. Similarly, the transformation between any two points in relative warp space (arrows in Fig. 1) can be expressed as a TPS function. This TPS function defines a displacement vector at every point of the cranial surface. The resulting spatial pattern of shape change is visualized as follows: for each point on the cranial surface, the displacement vector is decomposed into its normal and tangential components, relative to the local orientation of the surface. The normal component is colour coded—red and green indicates its orientation (inward and outward, respectively); colour intensity its magnitude. The tangential component is visualized as a vector field, indicating its direction and magnitude (see Figs 3 and 4).

Received 29 December 2000; accepted 26 June 2001.

1. Stringer, C. B. & Gamble, C. *In Search of the Neanderthals: Solving the Puzzle of Human Origins* (Thames and Hudson, London, 1993).
2. Krings, M. *et al.* A view of Neandertal genetic diversity. *Nature Genet.* **26,** 144–146 (2000).
3. Ovchinnikov, I. V. *et al.* Molecular analysis of Neanderthal DNA from the northern Caucasus. *Nature* **404,** 490–493 (2000).
4. Zollikofer, C. P. E., Ponce de León, M. S. & Martin, R. D. Computer-assisted paleoanthropology. *Evol. Anthropol.* **6,** 41–54 (1998).
5. Bookstein, F. L. *Morphometric Tools for Landmark Data* (Cambridge Univ. Press, Cambridge, 1991).
6. Rohlf, F. J. in *Contributions to Morphometrics* (eds Marcus, L., Bello, E. & García-Valdecasas, A.) 131–159 (Consejo superior de investigaciones científicas, Madrid, 1993).
7. Tillier, A.-M. in *The Human Revolution. Behavioural and Biological Perspectives on the Origins of Modern Humans* (eds Mellars, P. & Stringer, C. B.) 286–297 (Edinburgh Univ. Press, Edinburgh, 1989).
8. Rak, Y., Kimbel, W. H. & Hovers, E. A Neanderthal infant from Amud Cave, Israel. *J. Hum. Evol.* **26,** 313–324 (1994).
9. Dean, M. C., Stringer, C. B. & Bromage, T. G. Age at death of the Neanderthal child from Devil's Tower, Gibraltar and the implications for studies of general growth and development in Neanderthals. *Am. J. Phys. Anthropol.* **70,** 301–309 (1986).
10. Stringer, C. B., Dean, M. C. & Martin, R. D. in *Primate Life History and Evolution* (ed. DeRousseau, C. J.) 115–152 (Wiley-Liss, New York, 1990).
11. Williams, F. l. E. in *Neanderthals on the Edge* (eds Stringer, C. B., Barton, R. N. E. & Finlayson, J. C.) 257–267 (Oxbow Books, Oxford, 2000).
12. Zollikofer, C. P. E., Ponce de León, M. S., Martin, R. D. & Stucki, P. Neanderthal computer skulls. *Nature* **375,** 283–285 (1995).
13. Ponce de León, M. S. & Zollikofer, C. P. E. New evidence from Le Moustier 1: computer-assisted reconstruction and morphometry of the skull. *Anat. Rec.* **254,** 474–489 (1999).
14. Ponce de León, M. S. *Neanderthal Ontogeny: a Geometric Morphometric Analysis of Cranial Growth.* PhD thesis, Univ. Zürich (2000).
15. O'Higgins, P. & Jones, N. Facial growth in *Cercocebus torquatus*: an application of three-dimensional geometric morphometric techniques to the study of morphological variation. *J. Anat.* **193,** 251–272 (1998).
16. Rak, Y. The Neanderthal: a new look at an old face. *J. Hum. Evol.* **15,** 151–164 (1986).
17. Trinkaus, E. The Neandertal face: evolutionary and functional perspectives on a recent hominid face. *J. Hum. Evol.* **16,** 429–443 (1987).
18. Schwartz, J. H. & Tattersall, I. Significance of some previously unrecognized apomorphies in the nasal region of *Homo neanderthalensis*. *Proc. Natl Acad. Sci. USA* **93,** 10852–10856 (1996).
19. Rosas, A. Occurrence of Neanderthal features in mandibles from the Atapuerca-SH site. *Am. J. Phys. Anthropol.* **114,** 74–91 (2001).
20. Enlow, D. H. *Facial Growth* 3rd edn (Saunders, Philadelphia, 1990).
21. Lieberman, D. E., Pearson, O. M. & Mowbray, K. M. Basicranial influence on overall cranial shape. *J. Hum. Evol.* **38,** 291–315 (2000).
22. Franciscus, R. G. & Trinkaus, E. Determinants of retromolar space presence in Pleistocene *Homo* mandibles. *J. Hum. Evol.* **28,** 577–595 (1995).
23. Lieberman, D. E. in *Development, Growth and Evolution* (eds O'Higgins, P. & Cohn, M. J.) 85–122 (Linn. Soc. Lond., London, 2000).
24. Maureille, B. & Bar, D. The premaxilla in Neandertal and early modern children: ontogeny and morphology. *J. Hum. Evol.* **37,** 137–152 (1999).

25. Lieberman, D. E. Sphenoid shortening and the evolution of modern human cranial shape. *Nature* **393,** 158–162 (1998).
26. Lieberman, D. E., Ross, C. F. & Ravosa, M. J. The primate cranial base: ontogeny, function, and integration. *Yb. Phys. Anthropol.* **43,** 117–169 (2000).
27. Lieberman, D. E. & McCarthy, R. C. The ontogeny of cranial base angulation in humans and chimpanzees and its implications for reconstructing pharyngeal dimensions. *J. Hum. Evol.* **36,** 487–517 (1999).
28. Tattersall, I. & Schwartz, J. H. Morphology, paleoanthropology and Neanderthals. *New Anat.* **253,** 113–117 (1998).
29. Ubelaker, D. H. *Human Skeletal Remains. Excavation, Analysis, Interpretation* (Chicago Univ. Press, Chicago, 1978).
30. Zollikofer, C. P. E. & Ponce de León, M. S. Tools for rapid prototyping in the biosciences. *IEEE Comp. Graph. Appl.* **15,** 48–55 (1995).

Supplementary information is available on *Nature's* World-Wide Web site (http://www.nature.com) or as paper copy from the London editorial office of *Nature.*

Acknowledgements

We are grateful to R. D. Martin and P. Stucki for support of our research. C. B. Stringer's continuous help and advice is gratefully acknowledged. We thank C. Howell, J.-J. Jaeger, D. Lieberman, J. Schwartz and C. Pryce for valuable comments on an earlier version of this paper. We appreciate the help of the following curators in providing access to fossil specimens: J.-J. Cleyet-Merle, J.-M. Cordy, V. Kharitonov, M. Marinot, F. Menghin, R. Orban, I. Pap, Y. Rak, C. B. Stringer, B. Vandermeersch. We also thank the radiologists, physicists and technicians engaged in fossil computer tomography scanning: E. Berenyi, G. Bijl, P. Dondelinger, V. Dousset, W. Fuchs, S. Louryan, V. Makarenko, U. Shreter, N. Strickland and C. L. Zollikofer. This work was supported by the Swiss National Science Foundation and a habilitation grant of the Canton of Zurich.

Correspondence and requests for materials should be addressed to C.Z. (e-mail: zolli@ifi.unizh.ch).

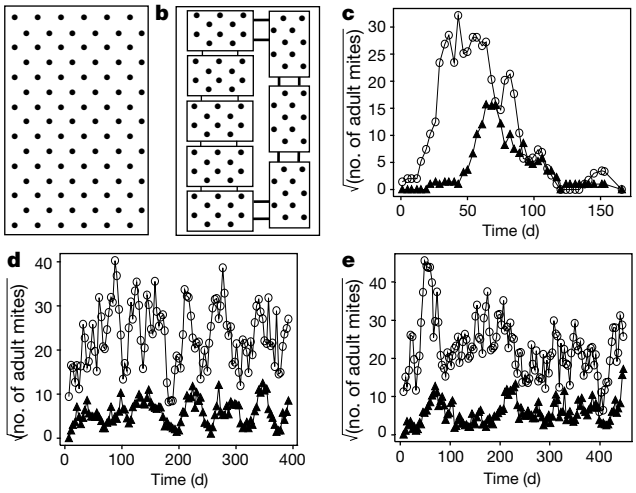

Figure 1 Experimental layouts and results. **a**, The single-island system consisted of a Styrofoam sheet with 90 embedded plants (filled circles) floating in a shallow tray of water. **b**, The metapopulation subdivided the sheet into 8 islands (10 plants per island) connected by cork bridges, with the space for 10 plants being lost. Replicate systems were housed simultaneously in the same environmental chamber, and given identical initial inoculations of mites. **c**, Fluctuations in total density of prey (open circles) and predatory (filled triangles) mites in the single-island experiment. **d**, **e**, Fluctuations in total density of prey (open circles) and predatory (filled triangles) miles in the two replicates of the metapopulation experiment.

Habitat structure and population persistence in an experimental community

Stephen P. Ellner*, Edward McCauley†, Bruce E. Kendall‡, Cheryl J. Briggs§, Parveiz R. Hosseini‖, Simon N. Wood¶, Arne Janssen#, Maurice W. Sabelis#, Peter Turchin☆, Roger M. Nisbet‖ & William W. Murdoch‖

* *Department of Ecology and Evolutionary Biology, Cornell University, Ithaca, New York 14853-2701, USA*
† *Ecology Division, Department of Biological Sciences, University of Calgary, Calgary T2N 1N4, Canada*
‡ *Donald Bren School of Environmental Science and Management; and*
‖ *Department of Ecology, Evolution and Marine Biology, University of California, Santa Barbara, California 93106, USA*
§ *Department of Integrative Biology, University of California, Berkeley, California 94720, USA*
¶ *School of Mathematical and Computation Sciences, University of St Andrews, Fife, Scotland KY16 9SS, UK*
# *Institute for Biodiversity and Ecosystem Dynamics, PO Box 94084, 1090 GB Amsterdam, The Netherlands*
☆ *Department of Ecology and Evolutionary Biology, University of Connecticut, Storrs, Connecticut 06269, USA*

Understanding spatial population dynamics is fundamental for many questions in ecology and conservation[1–4]. Many theoretical mechanisms have been proposed whereby spatial structure can promote population persistence, in particular for exploiter–victim systems (host–parasite/pathogen, predator–prey) whose interactions are inherently oscillatory and therefore prone to extinction of local populations[5–11]. Experiments have confirmed that spatial structure can extend persistence[11–16], but it has rarely been possible to identify the specific mechanisms involved. Here we use a model-based approach to identify the effects of spatial population processes in experimental systems of bean plants

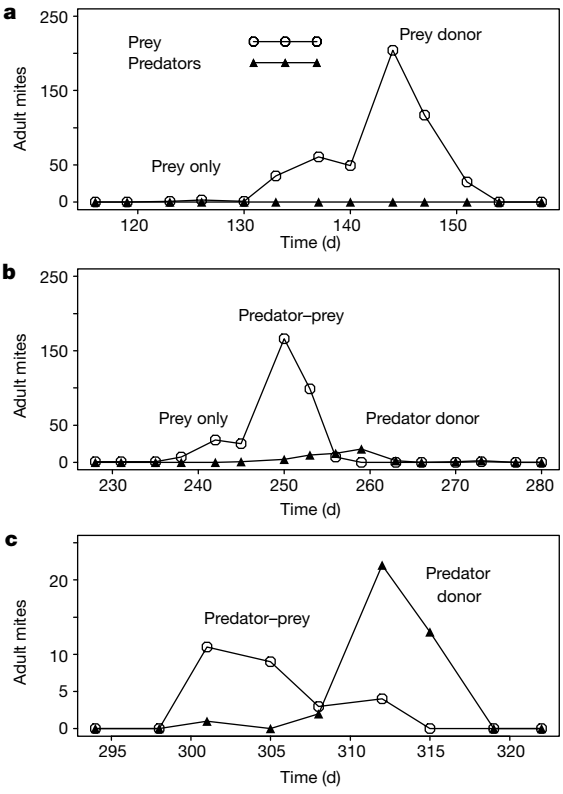

Figure 2 Examples of mite population dynamics on a single plant, from run B of the metapopulation experiment. **a**, A prey outbreak (plant 1, island 5) that was not discovered by predators. The three successively larger peaks in the prey density (days 126, 137 and 144) are the original colonizers, their offspring (counted when they become adults at age ~10 d), and offspring of the offspring. The rapid collapse of the outbreak is primarily due to emigration after exhaustion of the resource. **b**, A prey outbreak (plant 1, island 2) colonized by predators after several on-plant prey generations. Predators arrived too late to prevent growth of the prey population, and the outbreak terminated through exhaustion of the resource and prey emigration. **c**, A prey outbreak (plant 8, island 2) colonized by predators when prey densities were still low. The outbreak terminated through predators consuming all prey and then emigrating.